Topography Studies on the Membrane Interaction Mechanism of the Eosinophil Cationic Protein†

Marc Torrent,‡ Elisabet Cuyás,‡ Esther Carreras,‡,§ Susanna Navarro,‡ Olga López,|| Alfons de la Maza,|| M. Victòria Nogués,‡ Yana K. Reshetnyak,⊥ and Ester Boix*,‡

Departamento de Bioquímica i Biologia Molecular, Facultat de Ciències, Universitat Autònoma de Barcelona, 08193-Bellaterra, Spain, Departamento de Tensioactivos, Centro de Investigación y Desarrollo (CID), Consejo Superior de Investigaciones Científicas (CSIC), E-08034 Barcelona, Spain, and Physics Department, University of Rhode Island, Kingston, Rhode Island 02881

Received June 15, 2006; Revised Manuscript Received November 17, 2006

ABSTRACT: The eosinophil cationic protein (ECP) is an antipathogen protein involved in the host defense system. ECP displays bactericidal and membrane lytic capacities [Carreras et al. (2003) *Biochemistry 42*, 6636−6644]. We have now characterized in detail the protein−membrane interaction process. All observed fluorescent parameters of the wild type and single-tryptophan-containing mutants, as well as the results of decomposition analysis of protein fluorescence, suggest that W10 and W35 belong to two distinct spectral classes I and III, respectively. Tryptophan residues were classified and assigned to distinct structural classes using statistical approaches based on the analysis of tryptophan microenvironment structural properties. W10 belongs to class I and is buried in a relative nonpolar, nonflexible protein environment, while W35 (class III) is fully exposed to free water molecules. Tryptophan solvent exposure and the depth of the protein insertion in the lipid bilayer were monitored by the degree of protein fluorescence quenching by KI and brominated phospholipids, respectively. Results indicate that W35 partially inserts into the lipid bilayer, whereas W10 does not. Further analysis by electron microscopy and dynamic light scattering indicates that ECP can destabilize and trigger lipid vesicle aggregation at a nanomolar concentration range, corresponding to about 1:1000 protein/lipid ratio. No significant leakage of the vesicle aqueous content takes place below that protein concentration threshold. The data are consistent with a membrane destabilization "carpet-like" mechanism.

The eosinophil cationic protein (ECP)[1] is a human host defense ribonuclease with antipathogen capacities involved in inflammatory processes mediated by eosinophils (*1*, *2*). Antimicrobial properties have been reported for other RNase A family members: skin RNase (RNase 7) (*3*), eosinophil-associated RNases, and angiogenins (*4*). Moreover, a recent evolution study suggests that the family lineage might have started as an host defense protein (*5*). ECP bactericidal activity is not shared by the other eosinophil ribonuclease close homologue, the eosinophil-derived neurotoxin (EDN), nor their common EDN/ECP "ancestral" precursor (*6*). The mammalian RNase family study indicates that EDN and ECP emerged via a gene duplication and would have responded to unusual evolutionary constraints, which would have promoted an increased cationicity and cytotoxicity for ECP (*6*−*8*). ECP displays a reduced RNase activity for most common RNA substrates (*9*), although its RNase activity has been reported not necessary for the antibacterial capacity (*10*). The antimicrobial capacity has been linked to a membrane destabilization activity both in the RNase A family members and in eosinophil toxic proteins. Bovine seminal RNase, a RNase A family member that functions as a dimeric protein, with a described antitumor activity, can aggregate negatively charged vesicles and promote lipid mixing between bilayers and leakage of the vesicle aqueous content (*11*).

In mammalian blood cells, there is a wide array of cationic antimicrobial proteins and peptides, which contribute to the immune innate defense system (*12*, *13*). Eosinophils are important effector cells in the immune system (*14*). Eosinophil granule proteins participate in the inflammation disorders (*14*), and their deposits at the host epithelial tissues

† This work was supported by the Ministerio de Educación y Cultura (Grant BMC2003-08485-C02-01) and by the "Fundació La Marató de TV3" (TV3-031110). M.T. and E.C. are the recipients of predoctoral fellowships from the Generalitat de Catalunya, and S.N. is the recipient of a predoctoral fellowship from the Ministerio de Ciencia y Tecnología, Spain.

* To whom correspondence should be addressed: Departamento de Bioquímica i Biologia Molecular, Facultat de Ciències, Universitat Autònoma de Barcelona, 08193-Bellaterra, Spain. Telephone: 34-93-5814147. Fax: 34-93-5811264. E-mail: ester.boix@uab.es.

‡ Universitat Autònoma de Barcelona.

§ Present address: Oklahoma Medical Research Foundation, Oklahoma City, OK 73104.

|| Consejo Superior de Investigaciones Científicas (CSIC).

⊥ University of Rhode Island.

[1] Abbreviations: ECP, eosinophil cationic protein; EDN, eosinophil-derived neurotoxin; MBP, major basic protein; WT ECP, wild-type ECP; ANTS, 8-aminonaphthalene-1,3,6-trisulfonic acid; DPX, *p*-xylene-bis-pyridinium bromide; LUV, large unilamellar vesicles; DOPC, 1,2-dioleoyl-*sn*-glycero-3-phosphocholine; DOPG, 1,2-dioleoyl-*sn*-glycero-3-[phospho-rac-(1-glycerol)]; 6,7-diBrPC, 9,10-diBrPC, and 11,12-diBrPC, 1-palmitoyl-2-stearoyl-(6,7, 9,10, and 11,12)-dibromo-*sn*-glycero-3-phosphocholine; DLS, dynamic light scattering; FFEM, freeze-fracture electron microscopy.

10.1021/bi061190e CCC: $37.00
Published on Web 12/29/2006

contribute, among others, to the cutaneous disease pathologies (*15*). ECP levels in biological fluids are currently used for the diagnosis and monitoring of eosinophilia and other inflammatory disorders (*16*, *17*). Another eosinophil granule secretion protein involved in the antipathogen host defense activity, the major basic protein (MBP), has also been described to disrupt, aggregate, and fuse acidic liposomes (*18*). In fact, both eosinophil proteins, ECP and MBP, are able to permeabilize the bacteria outer and inner membranes (*19*).

Antimicrobial proteins and peptides in living organisms serve as an innate defense system, which works independent of prior exposure to pathogens and is complementary to the highly specific cell-mediated immune response (*12*, *20*). Antimicrobial proteins and peptides can act both at the bacteria cell wall and cytoplasmic membrane level. Because antibiotic resistance develops rapidly as soon as new agents are introduced, attempts to develop antimicrobial compounds with new mechanisms of action resulted in an increased interest in the role of antimicrobial proteins and peptides (*21*). A wealth of information is currently available related to the mechanism of action of antimicrobial peptides (*22*−*24*). However, little is known with respect to larger polypeptides, namely, small proteins, such as ECP.

Cationic and hydrophobic proteins are often involved in the innate immune host defense, displaying antipathogen activity against a wide range of species (*13*). The mode of action of antimicrobial proteins and peptides can act directly by lysis of the pathogen cell membrane (*25*). ECP cytotoxic and bactericidal activities correlate with its membrane disruption capacity and are dependent upon both surface-exposed hydrophobic and cationic residues (*26*, *27*). ECP also displays toxicity on the host epithelial tissues. In fact, ECP is cytotoxic for tracheal epithelium (*28*), and ECP deposits, related to tissue damage, are observed after eosinophil degranulation in inflammatory disorders (*29*). A local toxic action following eosinophil degranulation at the epithelium level could depend upon the protein direct interaction with cellular membranes and the intercellular matrix. ECP is indeed able to alter the multilamellar lipid structure of the pulmonary surfactant (*16*). In fact, studies on eosinophil-deficient mice suggest a critical role for eosinophils in airway remodeling (*30*).

To further characterize the ECP functional bactericidal mechanism, we have analyzed the mechanism of the protein−membrane interaction. Synthetic lipid vesicles have proven to be a good working model to analyze the protein activity on biological membranes. We describe here, by means of a variety of technical approaches, the events that take place when the protein encounters a lipid model system. Protein fluorescence spectroscopy and a method of decomposition of protein spectra were applied for the investigation of the protein−membrane interaction. Fluorescence properties of wild-type (WT) ECP and both W10 and W35 single mutants (Figure 1) have been analyzed in the absence and presence of large unilamellar vesicles (LUV). Experimental data have been compared to the theoretical calculation of the tryptophan (Trp) microenvironment properties from the protein atomic structures. Trp residues were classified and assigned to distinct spectral and structural classes using a statistical approach. We also investigated the Trp fluorescence quenching by using an external iodide quencher and brominated phospholipids to directly assess the protein binding to the lipid bilayer and estimate the depth of protein insertion. We have evaluated the ECP partial-insertion process into the lipid bilayer, together with the protein capacity to induce vesicle leakage and aggregation. The results are discussed with respect to the protein functionality.

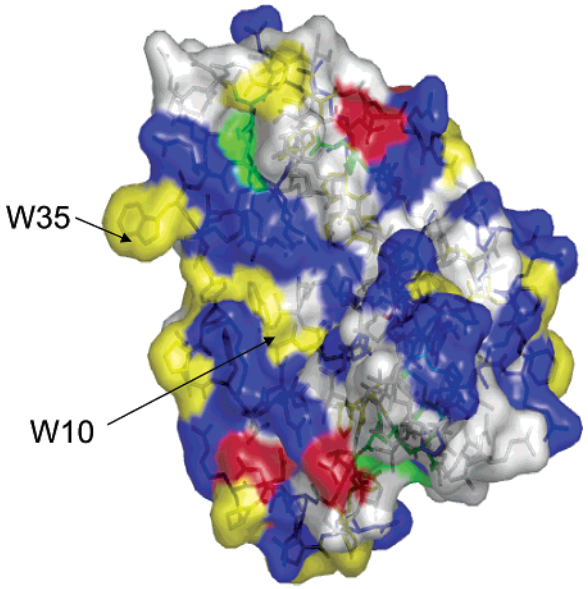

FIGURE 1: ECP surface molecular representation. The figure was drawn according to the ECP crystal structure coordinates, PDB entry code 1QMT (*34*). In this representation, hydrophobic, basic, acidic, and cysteine residues are colored in yellow, blue, red, and green, respectively. W10 and W35 locations are indicated. The figure was created with Pymol DeLano Scientific LLC.

EXPERIMENTAL PROCEDURES

Materials. 1,2-Dioleoyl-*sn*-glycero-3-phosphocholine (DOPC), 1,2-dioleoyl-*sn*-glycero-3-[phospho-rac-(1-glycerol)] (DOPG), 1-palmitoyl-2-stearoyl-(6,7, 9,10, and 11,12)-dibromo-*sn*-glycero-3-phosphocholine (6,7-diBrPC, 9,10-diBrPC, and 11,12-diBrPC) were from Avanti Polar Lipids, Birmingham, AL. *Escherichia coli* polar lipid extract, consisting of a mixture of phosphatidylethanolamine (67%), phosphatidylglicerol (23.2%), and cardiolipin (9.8%), was also obtained from Avanti Polar Lipids. 8-Aminonaphthalene-1,3,6-trisulfonic acid disodium salt (ANTS) and *p*-xylene-bis-pyridinium bromide (DPX) were from Molecular Probes, Invitrogen, Carlsbad, CA. Bovine pancreatic ribonuclease A, type XII-A, was purchased from Sigma-Aldrich.

Site-Directed Mutagenesis, Expression, and Purification of ECP Variants. WT ECP and W10K, W35A, and W35AR36A mutants were obtained from a human ECP synthetic gene (*9*). Mutants were constructed as described in ref *26*. Protein expression in the *E. coli* BL21(DE3) strain (Novagen, Madison, WI), folding of the proteins from inclusion bodies, and the purification steps were carried out as previously described (*9*).

Liposome Preparation. LUV of a defined size (about 200 nm) were prepared from a vacuum-drying lipid chloroform solution by extrusion through 800, 400, and 200 nm polycarbonate membranes. The lipid suspension was frozen and thawed several times prior to extrusion. Liposomes were obtained containing either DOPC/DOPG (3:2 molar ratio), pure DOPC, pure DOPG, or *E. coli* polar lipid extract. A 1

mM stock solution of liposome suspension in 10 mM Tris-HCl and 0.1 M NaCl at pH 7.4 was prepared. The final mean diameter of liposomes after the extrusion protocol was checked by dynamic light scattering (DLS). Calculated mean size values by DLS for DOPC, DOPG, DOPC/DOPG, and *E. coli* polar lipid liposomes were all in the range of 140−160 nm, with a polydispersity index of around 0.1.

Fluorescence Measurements. Trp fluorescence emission spectra were recorded at 280 and 295 nm excitation wavelengths. The excitation wavelength of 295 nm was used to obtain Trp emission data, free from the tyrosine signal. Slits were set at 2 nm for excitation and 5−10 nm for emission. Free Trp at an $OD_{280} = 0.36$ was used as an internal control. Emission spectra were recorded from 300 to 400 nm at a scan rate of 60 nm/min, in a 10 × 10 mm cuvette with stirring immediately after sample mixing. Protein spectra at 4 and 0.5 μM were obtained in the absence and presence of a 0.2 mM liposome suspension respectively, in 5 mM Tris-HCl and 0.1 M NaCl at pH 7.4 buffer, at 25 °C. Spectra in the presence of liposomes were corrected for light scattering, by substracting the corresponding LUV background. For each condition, three spectra were averaged. The fluorescence spectra were also calculated as a function of the frequency scale (wave number).

Quenching of Trp Fluorescence with Potassium Iodide (KI). Fluorescence quenching experiments were performed with KI. A 2 M KI solution, containing 1 mM sodium thiosulfate ($Na_2S_2O_3$) to prevent I^-_3 formation, was used as a stock solution. Aliquots of the quencher were added to the protein solution, in the presence and absence of liposomes. A potential effect because of an increase in the ionic strength was discarded by checking that wild-type and mutant protein spectra did not suffer any alteration when adding KCl up to 0.5 M, instead of KI. The fluorescence spectra were recorded using the following conditions: 5 mM Tris-HCl and 0.1 M NaCl at pH 7.4 buffer, at 25 °C, 0.5 μM protein concentration, and 0.2 mM liposome concentration, with an excitation wavelength at 280 nm and excitation and emission slits set to 5 nm. The area under the fluorescence spectra in the range from 320 to 380 nm was calculated. For each condition, three spectra were averaged. The data were analyzed according to the Stern−Volmer equation

$$\frac{F_o}{F} = K_{SV}[Q] + 1$$

where F_o is the initial fluorescence intensity, F is the intensity for each quencher concentration, [Q] is the quencher concentration, and K_{SV} is the Stern−Volmer constant. Data were represented by a Stern−Volmer plot, registering, for each KI concentration, the relative fluorescence intensities.

Decomposition of Trp Fluorescence Spectra. Decomposition of the fluorescence spectra of WT ECP in the absence and presence of 0.2 mM liposomes measured at different concentrations of KI was performed according to Burstein et al. (*33*). Briefly, the shape of each spectral component of protein fluorescence spectra on the frequency (wave number) scale was approximated by the uniparametric log-normal function (first, the fluorescence spectra were converted to the frequency scale from the wavelength scale $F_\nu = F_\lambda \lambda^2$)

$$I(\nu) = \exp\left\{-\frac{\ln 2}{\ln^2 \rho}\ln^2\left(\frac{a-\nu}{a-\nu_m}\right)\right\} \quad \text{at } \nu < a$$

where ν is the current wavelength number, ρ is the band asymmetry parameter

$$\rho = (\nu_m - \nu_-)/(\nu_+ - \nu_m)$$

and a is the function-limiting point position

$$a = \nu_m + (\rho(\nu_+ - \nu_-))/(\rho^2 - 1)$$

The intensities for the components (I_m) were calculated from the set of linear equations. The shape and position of spectral components remain unchanged at fluorescence quenching with water-soluble quenchers, and the change in intensity of individual components with quenching was checked to obey the Stern−Volmer law. The resolution into components was performed using simple fitting with mean-square criterion (SIMS) and phase-plot-based resolution using quenchers (PHREQ) algorithms. The spectra were independently fitted by one, two, or three components. Typical experimental noise of fluorescence spectra, which is about 0.5−1.5%, does not permit a sufficiently reliable decomposition for more than three spectral components. The criterion of attaining the best solution (a sufficient number of components) was the minimal root-mean-square differences (residuals) between theoretical and experimental spectra. For each ith component, the program output data contained the values of the spectral maximum position $\lambda_m(i)$, the percent contribution of the component into the area under the total spectrum $F(i)$, and the Stern−Volmer quenching constant $K_{SV}(i)$. The Stern−Volmer constants $K_{SV}(i)$ were calculated as slopes of the linear plots in coordinates $(A_o/A_c - 1)$ versus the quencher concentration, where A_o and A_c are the areas under emission component spectra, measured in the absence (A_o) and in the presence of the quencher in the concentration $c(A_c)$, respectively.

Structural Parameters of the Microenvironment of Trp Residues. Structural and physical parameters of the microenvironments of individual Trp residues were calculated from available atomic coordinates of ECP, PDB entry codes 1QMT (*34*) and 1DYT (*35*), and the ECP−2′,5′-ADP complex, PDB entry code 1H1H (*36*). The set of structural parameters was obtained within the ranges of 0−5.5 and 5.5−7.5 Å from each atom of the indole ring of each Trp. The following six structural parameters were considered: Acc, Acc1_7, Den, *B*, *R*, and *A*. Acc and Acc1_7 are the indole ring average relative accessibility to water and the mean accessibility of atom 1 (Nϵ1) and atom 7 (Cζ2) (without crystallization waters), respectively. We estimated the relative accessibility of each atom of indole moieties [especially, Nϵ1 (Acc1) and Cζ2 (Acc7) atoms] and the accessibility of indole ring as a whole (Acc) using the modified Lee and Richards approach (*37*). The relative accessibility was expressed as the percent ratio of the accessible area of an atom in a protein for the 1.4 Å spherical probe to that in free Trp. Den is the packing density, i.e., the number of neighbor atoms within the layers up to 7.5 Å around the indole ring. The parameter reflects the degree of burying of fluorophore into the protein matrix and/or the presence of hollow crevices in the structure. *B* is the

normalized crystallographic temperature factor (*B* factor). We used the averaged temperature *B* factors of "polar" atoms within 5.5 and 7.5 Å layers around indole atoms, normalized to the mean *B*-factor value of all Cα atoms in the crystal structure. *R* (*R* = Acc*B*) is the dynamic accessibility, which considers both the mobility of neighbor polar atoms and the accessibility of the indole ring to free highly flexible water molecules. The parameter *A* reflects the relative polarity of the environment within a sphere of 7.5 Å from fluorophores. The parameter is calculated as $A = S + (\mathrm{Acc}S)/100$, where *S* is the averaged percent portion of atoms of polar groups among all atoms in near and far layers.

Six structural parameters of the Trp residue were used for the calculation of two discriminant scores or roots by using package STATISTICA (StatSoft, Inc.). In other words, a six-dimensional space of parameters was concerted into an orthogonal two-dimentional space of roots and all further calculations (assignment of Trp residues to classes) were carried out in root coordinates.

Classification of Trp Residues. The classification of Trp residues to one of five classes (*31*, *38*) was performed on the basis of the calculation of probabilities of class assignment. Structural classes were constructed from the training set. The result of classification drastically depends upon the choice of training data set. For our training set, we choose proteins, where the assignment of spectral components to Trp residues was obvious and straightforward (see ref *31*). In the training set, we included the structural parameters of Trp residues of 24 proteins with up to 4 Trp fluorophore per protein. The probability (P_i) that Trp fluorophore (X_{new}) belongs to a particular class from the training set is proportional to the Mahalanobis distance (MD_i) between class centroid (μ) and the Trp residue

$$P_i = \frac{e^{-D_i^2/2}}{\sum_{j=1}^{n} e^{-D_j^2/2}}$$

$$D_i^2 = MD_i^2 + \ln|S_i| - 2\ln|q_i|$$

$$MD = \sqrt{(\mu - X_{new})S^{-1}(\mu - X_{new})'}$$

where *S* is a variance−covariance matrix and *q* is an *a priori* probability. The Mahalanobis distance takes into account the correlation between parameters by calculation of the variance−covariance matrix. Because we performed all calculations in space of orthogonal (noncorrelated) roots, the *S* matrix is converted into the diagonal matrix and the Mahalanobis distance is converted into the standard Euclidean metric. *A priori* probabilities are used to adjust posterior probabilities (P_i) by applying *a priori* knowledge of class distributions. *A priori* probabilities were driven from the fitting of the distribution of occurrence of the maximum position of spectral components (from ref *38*) by 5 G functions, which each represent five spectral classes with a maximum position at 308.0, 325.7, 331.7, 344.0, and 350.0 nm, respectively. The values of *a priori* probabilities for five classes were calculated as 0.01, 0.26, 0.22, 0.29, and 0.22, respectively.

Depth-Dependent Fluorescence Quenching Experiments Using Labeled Brominated Lipids. Quenching of protein Trp residues by brominated lipids was introduced to analyze the relative location of both W10 and W35 residues upon membrane interaction. LUV of DOPC/DOPG (3:2 molar ratio) were prepared as described above, containing either (6,7)-, (9,10)-, or (11,12)-Br_2PC. Brominated lipids were mixed at an increasing percentage from 20 to 80% with unlabeled DOPC/DOPG (3:2 molar ratio) vesicles. The fluorescence spectra were recorded using the following conditions: 10 mM Tris-HCl at pH 7.4 buffer, at 25 °C, 0.5 μM protein concentration, and 0.2 mM liposome concentration, with an excitation wavelength of 280 nm, excitation and emission slits set to 2 and 10 nm, respectively, and a 10 × 10 mm cuvette with continuous stirring. The background corresponding to the vesicles without the protein was substracted. The fluorescence emission spectra were calculated as a function of the frequency scale (wave number) and fitted to a quadriparametric log-normal function. The area under the fluorescence spectra in the range from 320 to 380 nm was calculated. For each condition, three spectra were averaged. Vesicle samples were incubated with the protein, and the fluorescence spectra was recorded. The quenching efficiency of brominated lipids on protein Trp fluorescence was assayed by calculating the area under the fluorescence spectra in the range of 320−380 nm. Data were normalized to the intensity in the absence of quenching. Relative fluorescence intensities (F_0/F) were compared. To calculate the depth of insertion of the protein in the lipid bilayer, the distribution analysis (DA) was employed (*39*). Depth-dependent fluorescence quenching profiles using the DA were fitted to data, using the equation below

$$\ln\frac{F_0}{F(h)}c(h) = \frac{S}{\sigma\sqrt{2\pi}}\exp\left[-\frac{(h - h_m)^2}{2\sigma^2}\right]$$

where F_0 is the fluorescence intensity in the absence of the quencher, $F(h)$ is the intensity in the presence of the quencher at the distance *h* (in angstroms) from the bilayer center, and h_m is the average location depth of the Trp residues. The depth-dependent fluorescence quenching profiles are fitted with a Gaussian function, where σ denotes the dispersion, related to the in-depth distribution of the chromophores, *S* is the area under the quenching profile, related to the ability of quenching of Trp fluorescence, and *h* is the average bromine distance from the bilayer center. The average bromine distances from the bilayer center based on X-ray diffraction are considered to be 10.8, 8.3, and 6.3 for (*6*,*7*)-, (*9*,*10*)-, and (*11*,*12*)-Br_2PC, respectively (*40*). Equal concentrations of the brominated lipids have been used; therefore, the $c(h)$ value is equal to 1.

ANTS/DPX Liposome Leakage Assay. The ANTS/DPX liposome leakage fluorescence assay was performed as described previously (*26*). Briefly, a unique population of LUV of *E. coli* polar lipid extract was obtained containing 12.5 mM ANTS, 45 mM DPX, 20 mM NaCl, and 10 mM Tris-HCl at pH 7.5. Unencapsulated material was separated from the vesicles by gel filtration on Sephadex G-25 (Amersham Pharmacia Biotech) using 20 mM Tris-HCl at pH 7.5 containing 0.1 M NaCl as an elution buffer. The lipid concentration was determined by a colorimetric assay method for free and phosphorylated glyceric acids (*41*). The ANTS/

DPX liposome suspension was diluted to a 30 μM final concentration and was incubated at room temperature in the presence of the protein. The leakage activity was assayed at different protein concentrations by following the release of the liposome content. Fluorescence was measured using a 386 nm excitation wavelength and 535 nm emission wavelength. Slits were set at 5 and 10 nm for excitation and emission, respectively. Cutoff filters for excitation and emission wavelengths were set at 250−395 and 430−1100 nm, respectively. The percentage of leakage (% L) produced by the proteins after 1 h of incubation with the liposomes was calculated with the following equation: (% L) = 100-($F_p - F_0$)/($F_{100} - F_0$), where F_p is the final fluorescence intensity after the addition of the protein (1 h), F_0 and F_{100} are the fluorescence intensities before the addition of the protein and after the addition of 0.5% Triton X-100. For each protein concentration, three calculated leakage values were averaged.

DLS. Changes in liposome population were analyzed by DLS using a Malvern 4700 photon correlation spectrometer (Malvern Instruments, Malvern, U.K.). An argon laser (λ = 488 nm) was used to cover the wide size range involved. The hydrodynamic radius measurements were always carried out at a reading scattering angle of 90°. All experiments were thermostatically controlled. The intensity measurements were recorded; the data were processed; and the hydrodynamic diameter (HD), the polydispersity index (PI), and the total number of counts were calculated. The analysis of the data was performed using CONTIN software provided by Malvern Instruments, and the calculated values were checked according to the REPES analysis (*42*). The vesicle size distribution of liposomes was determined at different lipid/protein molar ratios. The incubation buffer was 10 mM Tris-HCl and 0.1 M NaCl at pH 7.4. Measurements were performed at 25 °C, a 0.2 mM final liposome concentration, and a protein concentration ranging from 10 nM to 2 μM.

Freeze-Fracture Transmission Electron Microscopy (FFEM). A morphological study on the changes in the liposome population was followed by FFEM according to the protocol previously reported (*43*). Vesicles prepared with *E. coli* polar lipid extract at a 5 mM lipid concentration were incubated at room temperature with 2.5 or 5 μM ECP in 20 mM Tris-HCl and 0.1 M NaCl at pH 7.5 for 1, 15 and 30 min. A freeze-fracture electron microscopy study was done according to the procedure previously described (*44*). The suspension was sandwiched between two copper platelets using a 400-mesh gold grid as a spacer. The samples were frozen in a Leica EM CPC cryopreparation system (Leica, Vienna, Austria) using propane immersion, at −189 °C, and fractured at −150 °C and 10^{-8} mbar in a Bal-Tec BAF 060 freeze-etching system (BAL-TEC, Liechtenstein). The replicas were obtained by unidirectional shadowing with 2 nm of Pt/C and 20 nm of C, and they were floated on distilled water during 5 min. The replica were observed at a 10 000−100 000× magnification range in a Jeol J1010 electron microscope at 80 kV. For each condition, three cryofixations were carried out and three freeze-fracture replicates were obtained from each. On average, about 50 freeze-fractured transmission electron micrographs were taken. The mean size and morphological shapes of the liposome population were analyzed. Size estimation of the visualized liposomes was performed only on the liposomes that were fractured on their equatorial plane.

RESULTS

Protein Fluorescence Properties in the Absence and Presence of Liposomes. Trp fluorescence spectroscopy is a widely used method to study protein structure and dynamics. We have applied this technique to investigate conformational changes, which occur in ECP during its interaction with lipid bilayers. First, we compared the fluorescence spectra recorded at 280 and 295 nm excitation wavelengths. The results indicated that the contribution of four tyrosine residues to the total fluorescence signal was negligible. Therefore, all spectra were recorded at 280 nm of excitation.

ECP is a 15 kDa protein containing two Trp residues W10 and W35 (Figure 1). We have analyzed the fluorescence properties of the WT ECP protein and single-Trp-containing mutants in the absence and presence of synthetic and natural lipids (Figure 2). To study the contribution of the W10 residue in total protein fluorescence, mutants lacking the other Trp (W35) were constructed (W35A and W35AR36A mutants). Likewise, to analyze W35 contribution, the W10 residue was substituted (W10K mutant). Also, we applied the fluorescence decomposition method (*33*) to reveal individual spectral components from the total emission spectra of ECP. The maximum position of fluorescence spectra of WT ECP and its mutants in the absence and presence of liposomes (see Table 1) correlates very well with the values of spectral parameters obtained as a result of decomposition analysis (Table 2) (note that we used corrected spectra in the decomposition analysis). The fluorescence data of W35A and W10K correspond to the first and second spectral components, respectively. On the basis of the fluorescent properties of mutant proteins and calculated spectral components, W10 and W35 could be assigned to the spectral classes I and III, respectively.

The interaction of ECP with the lipid bilayer leads to changes in the protein spectral properties: a blue shift of the emission spectrum in the presence of liposomes (Figure 2 and Table 1). The mutant keeping only W35 (W10K) and the second spectral component (Table 2) display a blue shift greater than ECP, whereas the constructs keeping only W10 (W35A) and first spectral component show a very small shift (Figure 2 and Tables 1 and 2). Results obtained with the W35AR36A double mutant are similar (data not shown). The blue shift recorded for ECP in the presence of liposomes is also accompanied by an increase in the fluorescence intensity (Figure 2). The results indicate that most of the changes in the ECP fluorescence during protein interactions with the lipid bilayer are contributed by W35. We can deduce that W35 would be in close contact with the phospholipid bilayer during the protein−membrane association process. Analyzing the protein fluorescence spectra shift in the absence and presence of liposomes of distinct lipid composition, we register significant differences (Table 1). By monitoring of the Trp fluorescence changes in ECP, we observe the lack of protein interaction with pure neutral lipid bilayers and the protein increasing affinity for DOPC/DOPG and *E. coli* polar lipid extracts.

Theoretical Analysis of Structural Parameters of Protein Trp Microenvironments. In parallel to the spectral analysis,

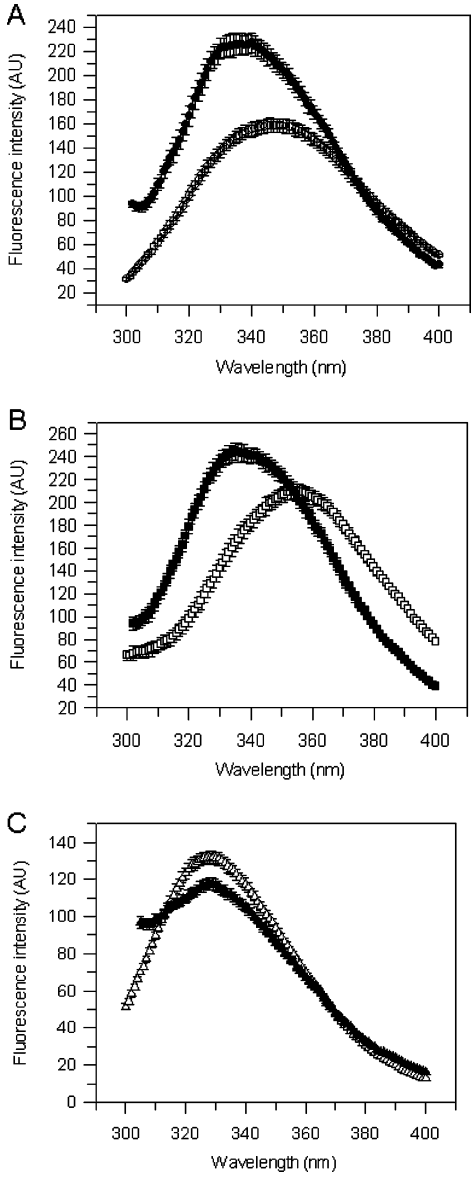

FIGURE 2: Comparison of the fluorescence emission spectra of (A) WT ECP, (B) W10K, and (C) W35A mutants in the absence (○, □, and △) and presence (●, ■, and ▲) of 3:2 DOPC/DOPG liposomes, as described in the Experimental Procedures. Protein and lipid final concentrations were 0.5 and 200 μM, respectively. For each condition, three spectra were averaged.

Table 1: Maximum Position of Protein Fluorescence Spectra of WT ECP and W10K and W35A Mutants in the Absence and Presence of Liposomes[a]

	maximum position of emission spectra in wavelengths (nm)		
	ECP	W35A	W10K
without liposomes	344.5 ± 0.1	326.1 ± 0.1	351.2 ± 0.1
DOPC	342.4 ± 0.1	321.2 ± 0.1	348.6 ± 0.2
3:2 DOPC/DOPG	338.7 ± 0.1	327.6 ± 0.1	339.2 ± 0.1
E. coli polar lipid extract	336.3 ± 0.3	327.1 ± 0.2	331.9 ± 0.3

[a] The fluorescence emission spectra were recorded at a 280 nm excitation wavelength. The data were fitted with a log-normal function as described in the Experimental Procedures.

we performed the examination of the structural properties of the microenvironment of the two Trp residues of ECP from atomic structures by using the algorithm described previously (*31*). The data are summarized in Table 3. The two molecules of the ECP crystallographic dimer structure [PDB entry code 1DYT (*35*)] show some differences on the structural parameters for the W10 residue microenvironment. In fact, molecular dynamics simulation studies on the ECP crystallographic dimer (*46*) indicate that main significant differences between the two units lie mainly at the ECP N terminus. Therefore, we have compared the structural parameters of the alternate positions in both dimer molecules (Table 3). A comparison of both available crystallographic forms also indicates that W35 in the 1DYT structure (*35*) is more solvent-exposed than in the 1QMT form (*34*). This is consistent with a higher indole ring solvent accessibility (Acc), normalized dynamic accessibility (*R*), and environment relative polarity (*A*). However, interpretation of the data must bear in mind the differences in the crystal data resolution and the fact that the 1DYT crystal has two molecules in the asymmetric unit and W35 is located in a hydrophobic patch at the dimer interface. Analysis of the protein interfaces was evaluated by the buried area percentage calculated with the web-server software Protein Interfaces, Surfaces, and Assemblies (PISA) version 1.02 (*45*).

Six structural parameters, which are known to correlate with spectral properties (*31*), of the two Trp residues of ECP are presented in Table 3. These parameters are used to establish the assignment of Trp residues to the discrete classes based on the comparison with the training set (see the detailed description of the classification procedure in the Experimental Procedures). W35 was assigned to class III with high accuracy, and W10 was allocated to class I based on the examination of the structural properties. Trp fluorophores, which belong to class I, are usually buried in the protein matrix. The density of protein atoms is rather high, and the environment is relatively nonpolar and nonflexible around the fluorophores of class I (*33*). This spectral form has a maximum of emission at about 330 nm, an approximated full width at half-maximum intensity of 50 nm, and no vibrational structure. Spectral form III (class III) contains Trp residues fully exposed to highly mobile water molecules. This spectral form has a fluorescence maximum at 348−350 nm and an approximated full width at half-maximum intensity of 60 nm; a spectrum very similar to the spectrum of free Trp in solution. This class is rather unusual in native proteins but very common in denatured proteins or short unstructured peptides.

The presence of potential intramolecular fluorescence quenchers as described (*31*) was also evaluated by analyzing all of the protein neighbor atoms in the vicinity of both W10 and W35 indole rings, located in the near (up to 5.5 Å) and far (5.5−7.5 Å) layers. There are several potential fluorescence quenchers of W10 (located at a distance of less than 5.5 Å), which are Nϵ, Nη_1, and Nη_2 atoms of Arg 1 and 34, the Nζ atom of Lys 38, and Oϵ_1 and Nϵ_2 atoms of Gln 14. Among the potential quenchers of emission of W35, we can point out nitrogen atoms of the side chain of Arg 36. These finding are in good agreement with the contribution of the spectral components in total intensity; the fluorescence of the short-wavelength component is about 2 times lower than the emission of the long-wavelength component originated from W35 (see Figure 2 and Table 2).

Quenching of the Protein Fluorescence by KI. Fluorescence quenching results using KI as an external ionic soluble quencher of Trp emission were obtained in the presence and

Table 2: Maximum Position (λ_{max}, nm), Contribution (F, %) and Stern−Volmer Constants (K_{SV}, M^{-1}) of Spectral Components Obtained as a Result of the Decomposition Analysis of WT ECP in the Absence and Presence of DOPG Liposomes[a]

	first component (W10)			second component (W35)		
	λ_{max} (nm)	F (%)	K_{SV} (M^{-1})	λ_{max} (nm)	F (%)	K_{SV} (M^{-1})
ECP	328.9 ± 2.1	31.1 ± 4.3	4.2 ± 1.6	344.2 ± 3.2	68.9 ± 4.3	14.2 ± 1.6
ECP plus DOPG	327.5 ± 3.1	34.8 ± 1.4	3.5 ± 2.0	339.5 ± 2.9	65.2 ± 1.4	3.1 ± 2.2

[a] The Stern−Volmer constant for Trp quenching of free Trp in solution is 14.6 M^{-1}.

Table 3: Structural Parameters and Classification of Trp Residues of ECP[a]

	Acc	Acc1_7	Den	*B*	*R*	*A*	probability of classification
Trp10, 1QMT[b]	8.9	23.8	123	0.934	8.3	36.9	79% class I
Trp35, 1QMT	67.9	69.9	26	0.935	63.4	73.7	100% class III
Trp10,[c] 1DYT[d]	6.8	17.9	142	1.106	7.4	42.5	77% class I
Trp10, 1DYT; chain A	5.3	12.2	147	1.134	6.05	42.9	67% class I
Trp10, 1DYT; chain B	8.2	23.5	137	1.079	17.6	42.2	74% class I
Trp35,[c] 1DYT	84.1	99.1	36	1.473	123.9	98.3	100% class III
Trp35, 1DYT; chain A	84.0	100	37	1.614	135.6	109.9	100% class III
Trp35, 1DYT; chain B	84.3	98.2	35	1.333	112.3	86.7	100% class III
Trp10, 1H1H[e]	8.5	21.7	133	0.984	8.3	40.3	78% class I
Trp35, 1H1H	67.3	67.9	27	0.862	58.0	71.5	100% class III

[a] The calculation of structural parameters and classification analysis were performed using the algorithms described in ref *31*. Acc is indole ring average accessibility. Acc1_7 is a mean accessibility of atom 1 (Ne1) and atom 7 (Cz2) (without crystallization waters). Den is the packing density. *B* is the normalized temperature factor (*B* factor). *R* is the normalized dynamic accessibility. *A* is the environment relative polarity calculated from the percentage of polar atoms, within a sphere of 7.5 Å of the fluorophore. Trp residues were classified and assigned to distinct classes using an algorithm as described in ref *31*. [b] PDB entry code 1QMT (*34*). [c] The mean values of chains A and B. [d] PDB entry code 1DYT (*35*). [e] PDB entry code 1H1H (*36*).

absence of liposomes. Data were fitted to the Stern−Volmer equation. Quenching by the iodide anion (I^-) is considered to be limited to protein surface Trp (*47*, *48*). For mutant proteins in the absence and presence of liposomes, deviation from linearity was minimal and approximate K_{SV} values could be determined from initial slopes (Figure 3). However, the Stern−Volmer plots for WT ECP in the absence and presence of lipids exhibit nonlinear behavior, which is a characteristic for multi-Trp proteins with several emitting species. Indeed, the spectral properties of Trp residues are different, and they represent two distinct species in the WT protein. The Stern−Volmer constants for each Trp in WT ECP were calculated by decomposition analysis, and data are presented in Table 2. The quenching data are in very good agreement with other spectral and structural analysis. The results confirm that, when the protein is in solution, W10 is mostly buried, while W35 is accessible to the solvent, as already observed in the ECP three-dimensional crystallographic structure (Figure 1) (*34*) and evaluated by calculating the solvent-accessible surface area (SASA) for both Trp residues (*26*). The Stern−Volmer plots for WT ECP and the W10K mutant in the absence and presence of DOPG liposomes were also compared (Figure 3B). The recorded KI quenching effect for W10K is similar to the one registered for the wild-type protein. Upon incubation of the W10K mutant in the presence of DOPG liposomes, a reduction of the K_{SV} is recorded ($K_{SV} = 9.7\ M^{-1}$ in absence of liposomes, and $K_{SV} = 1.14\ M^{-1}$ in presence of liposomes). A similar behavior was obtained by using decomposition analysis. The Stern−Volmer constant of the first (blue-shifted) spectral component is not affected by the presence of anionic lipids. However, the Stern−Volmer constant of the long-wavelength component (corresponding to W35) decreased considerably (Table 2). The results would suggest that the solvent-exposed W35 residue changes its microenvironment when the protein interacts with the membrane. On the other hand, no changes in the quenching profile for WT ECP in the presence or absence of DOPC vesicles (Figure 3C) corroborated the lack of interaction of the protein Trp residues with neutral lipids.

Depth-Dependent Fluorescence Quenching Experiments Using Labeled Brominated Lipids. Depth-dependent fluorescence quenching of ECP Trp residues was performed using LUV prepared with dibrominated phospholipids at several depth positions. Brominated lipids were mixed at a 20−80% molar ratio with 3:2 DOPC/DOPG lipids. The degree of membrane penetration of ECP was followed by analyzing the quenching effect of brominated lipids on both W10 and W35 fluorescence. The synthesized brominated PC derivatives, which do not contain double bonds, form bilayers of equal thickness and properties similar to lipids with one unsaturated bond, because bromine is a small molecule that does not drastically disturb the lipid bilayer (*49*), and the bulkiness of the bromine atoms has similar effects on lipid packing as a cis double bond (*50*).

The quenching efficiency of brominated lipids on protein Trp fluorescence was compared for WT ECP and both Trp mutants (Figure 4). The fluorescence quenching results indicate that ECP can partially insert into the lipid bilayer. Results on the wild-type protein were compared with both single Trp mutants (W10K and W35A). In all cases, the spectra were recorded when the assay mixture was equilibrated and no changes in the fluorescence signal were detectable. Parts A and B of Figure 4 show the Stern−Volmer plots for the Trp quenching of WT ECP and W10K and W35A mutants by brominated lipids. We observe that a comparable quenching profile is obtained for ECP and the W10K mutant, while no significant changes are detectable for the W35A mutant. The data indicate that most of the quenching effect on ECP fluorescence is due to the contribution of the exposed W35. The recorded quenching slopes are comparable for the 9,10- and 6,7-brominated lipids, while the brominated lipid labeled at 11,12 positions presents a

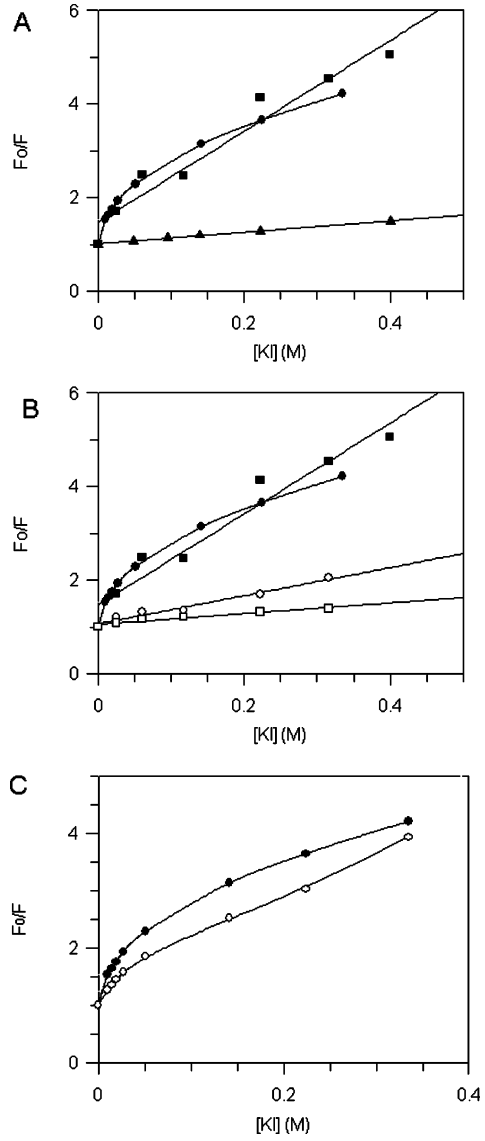

FIGURE 3: Stern−Volmer plots of ECP emission fluorescence quenching by KI in the absence and presence of lipid vesicles. (A) Fluorescence quenching by KI of (●) ECP, (■) W10K, and (▲) W35AR36A mutants. (B) Fluorescence quenching by KI in the absence (●, ■, and ▲) and presence (○, □, and △) of DOPG lipid vesicles for ECP (○) and (□) W10K mutant. (C) Fluorescence quenching by KI in the absence (●, ■, and ▲) and presence (○, □, and △) of pure DOPC lipid vesicles for ECP. Protein and lipid final concentrations were 0.5 and 200 μM, respectively.

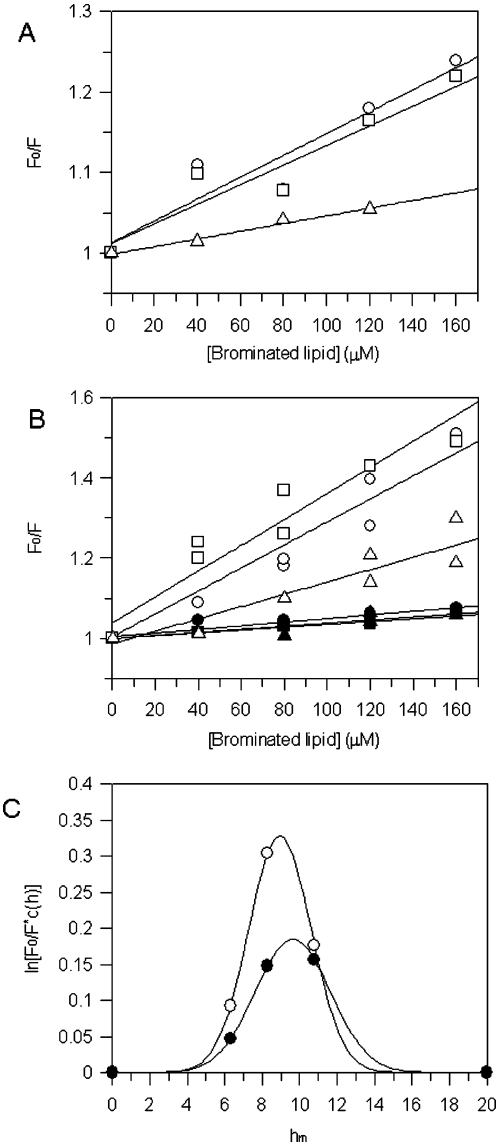

FIGURE 4: Stern−Volmer plots for the depth-dependent quenching of Trp fluorescence for (A) WT ECP and (B) W10K (○, □, and △) and W35A mutants (●, ■, and ▲). Liposomes containing 3:2 DOPC/DOPG lipids were mixed with an increasing molar ratio of (6,7)-Br_2PC (□), (9,10)-Br_2PC (○), or (11,12)-Br_2PC (△). Assay conditions were 0.5 μM final protein concentration and 200 μM liposome concentration. (C) Depth-dependent fluorescence quenching profile of WT ECP (●) and W10K (○) calculated by the DA to visualize the changes in fluorescence Trp chromophores (F), normalized to its value in the absence of quenching (F_0), when the quencher is present at certain depths in the bilayer. h_m is the average location depth of the Trp residues.

much more reduced quenching capacity. Therefore, the data suggest that none of the protein Trp is inserted deeply in the lipid bilayer. To calculate the depth of insertion of the protein in the lipid bilayer, the DA was employed. The DA method describes the quenching profile by a Gaussian function, where h_m is an average location depth of the Trp residues, σ denotes the dispersion, related to the in-depth distribution of the fluorophores, and S is the area under the quenching profile. The DA calculation, dependent upon three parameters, is considered to be more robust and less dependent upon uncertainty in the local concentration of quenching lipids (because of the protein-shielding effect or nonideal lipid mixing), incomplete binding, or the existence of multiple conformations of membrane-bound protein (*39*). We can estimate that in the assayed conditions most of the protein is bound to the membranes. In any case, the DA calculation allows an estimate of Trp insertion into the membrane even if a fraction of the protein is not bound to the membrane (*39*). In the assayed working conditions, we can rule out a main contribution of a significant transleaflet quenching, because of the protein membrane destabilization activity. The quenching profiles for ECP and W10K are illustrated in Figure 4C. Depth-dependent fluorescence quenching profiles calculated by the DA, represented by a Gaussian function, indicate a Trp depth location of about 9−10 Å from the bilayer center, as calculated for both WT ECP and the W10K mutant. An average depth location from the lipid bilayer center of about 9 Å can be estimated for

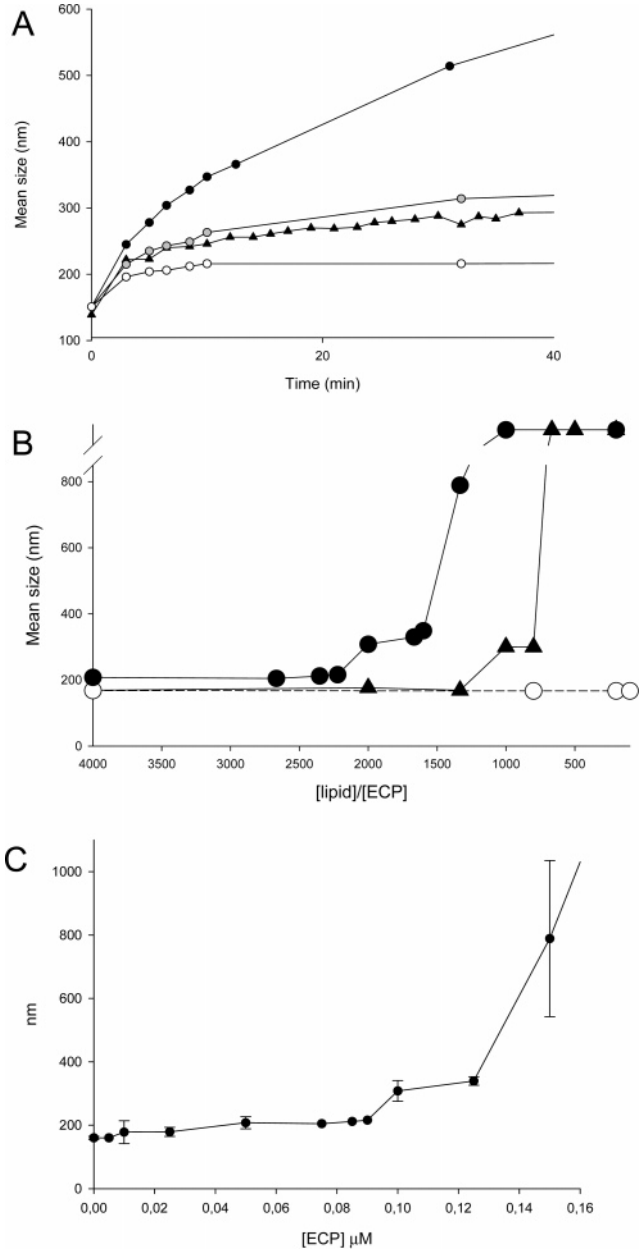

FIGURE 5: Evolution of the liposome population mean size upon incubation with ECP, evaluated by DLS. (A) Time-course recording using *E. coli* polar lipid extract at (○) 0.09 μM, (shaded circles) 0.12 μM, (●) 0.15 μM, and (▲) 3:2 DOPC/DOPG lipids at 0.2 μM. (B) Changes in the mean size of the liposome population as a function of the lipid/protein ratio. Liposomes at 200 μM final concentration of distinct lipid composition were assayed: (●) *E. coli* polar lipid extract, (▲) 3:2 DOPC/DOPG, and (○) DOPC. (C) Mean size of the liposomes as a function of the final protein concentration up to 0.15 μM, using *E. coli* polar lipid extract. Final values after 1 h of incubation at room temperature are taken. Mean size values higher than 1000 nm correspond to a polydispersity index value close to 1, indicating a great dispersion of the vesicle population, and cannot be measured accurately.

the W35 residue, while W10 would not insert into the membrane significantly.

DLS. The process of the ECP interaction with the membrane has been further analyzed by DLS (Figure 5). DLS measurements show that the ECP interaction with liposomes lead to large structures, which would correspond to aggregation and/or fusion of lipid vesicles. The effect of the protein interaction with the vesicles is detectable immediately after the lipid/protein mixture (Figure 5A). A time course has been registered at several protein concentrations, ranging from 0.09 to 0.15 μM, for *E. coli* polar lipid extracts, and 0.2 μM, for DOPC/DOPG liposomes. We are observing a gradual increase on the calculated liposome population mean size value as a function of time. A parallel increase in the polydispersity index up to 1 is also observed (data not shown), suggesting that the mean size increase is concomitant to an increase in the population hetereogeneity, which would be mainly due to vesicle aggregation. The aggregation capacity is strongly dependent upon the assayed protein range concentration, showing a sigmoidal response. A sigmoidal dependence on the mean size liposome population as a function of the protein concentration suggests a cooperative process. Figure 5B shows the evolution on the mean size of the vesicle population as a function of the lipid/protein molar ratio. The ECP activity was assayed on pure DOPC, mixed 3:2 DOPC/DOPG, and *E. coli* polar lipid extract liposomes. No detectable activity is observed for neutral DOPC liposomes at the assayed concentration range, even at a 100 lipid/protein ratio. When the protein concentration is increased up to a threshold value, between 100 and 200 nM (5C), corresponding to about 1:1300 protein/lipid molar ratio for *E. coli* lipid liposomes and 1:800 for 3:2 DOPC/DOPG liposomes, the mean size value of the liposome population increases dramatically, leading to liposome aggregation, visual sample turbidity, and sample precipitation. Mean size values higher than 1000 nm correspond to a polydispersity index close to 1, indicating a great dispersion of the vesicle population, and cannot be measured accurately. In fact, the highly polydisperse samples correspond to a high degree of liposome aggregation, as corroborated by their visual inspection.

Table 4: Percentage of Leakage (% *L*) of the ANTS/DPX Liposomes Produced by the Proteins after 1 h of Incubation at Room Temperature[a]

lipid/ECP ratio	[ECP] (nM)	% *L*	lipid/ECP ratio	[ECP] (nM)	% *L*
4000	7.5	1.2	300	100	3.9
1300	23	2.1	200	150	10.6
900	33	1.5	100	300	11
600	50	2.3	50	600	23
400	75	3.4			

[a] The percentage of leakage (% *L*) was calculated with the following equation: (% *L*) = $100(F_p - F_0)/(F_{100} - F_0)$, where F_p is the final fluorescence intensity after the addition of the protein (1 h) and F_0 and F_{100} are the fluorescence intensities before the addition of the protein and after the addition of 0.5% Triton X-100. For each condition, three calculated leakage values were averaged.

ANTS/DPX Liposome Leakage Assay. We have evaluated the protein capacity to trigger the liposome leakage content by the ANTS/DPX fluorescence assay. ECP can promote the lipid bilayer destabilization, and the release of the liposome-entrapped content is detectable from a threshold protein concentration. No leakage activity, under equivalent assay conditions, was detectable for both RNase A and EDN, while a 100% leakage capacity was reached for ECP up to a lipid/protein ratio of 7 (corresponding to a 5 μM protein final concentration), using 3:2 DOPC/DOPG liposomes (*26*). Table 4 includes the calculated leakage percentages at several lipid/protein ratios. No significant liposome content leakage is taking place below a 100 nM protein concentration. A

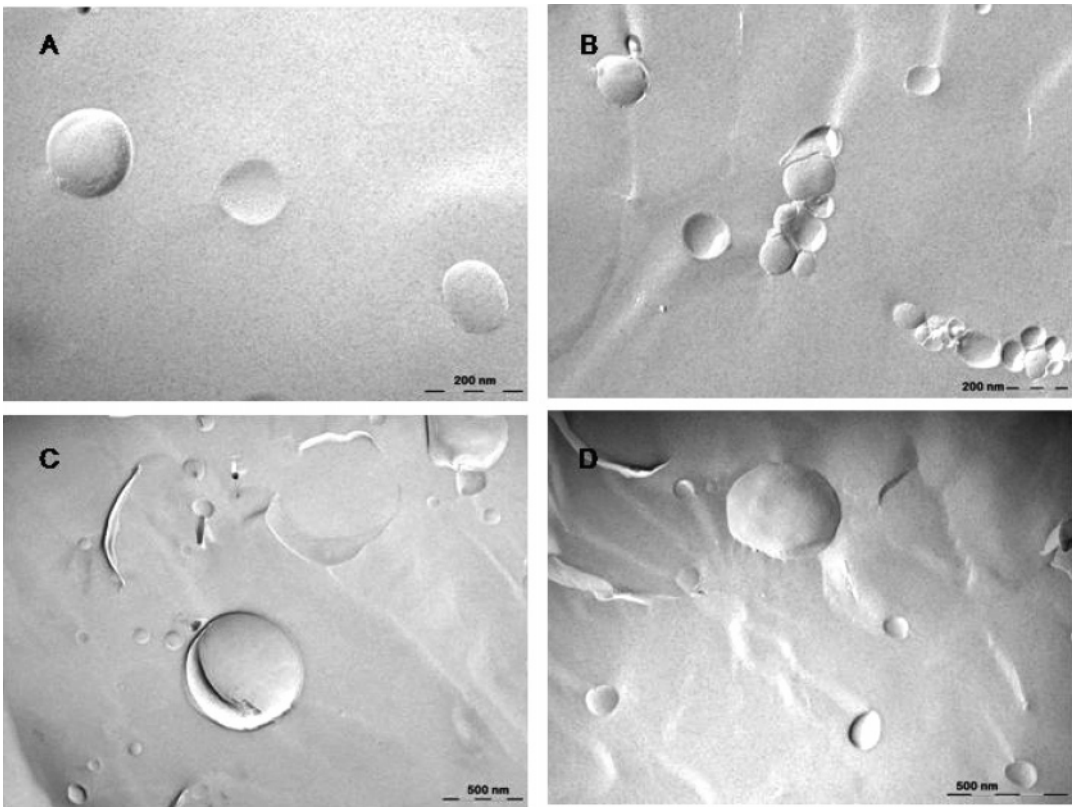

FIGURE 6: Freeze-fracture electron micrographs of *E. coli* lipid liposomes incubated with ECP, at a 2000 lipid/protein concentration ratio. Liposomes prepared with *E. coli* polar lipid extract at 5 mM lipid concentration were incubated at room temperature with 2.5 μM of ECP in 20 mM Tris-HCl and 0.1 M NaCl at pH 7.5. Freeze-fracture replicas of free liposomes (A) and incubated with ECP for 30 min (B−D). The reference size scale is included inside the micrographs.

clear vesicle aggregation is detected before any considerable leakage of the liposome-entrapped content takes place (see also parts A and C of Figure 5). Therefore, the protein would trigger the liposome population aggregation before any membrane-disruption or pore-formation process. Higher protein concentrations, where a clear leakage is observed, correspond to liposome aggregation, visible turbidity, and sample mixture precipitation. Therefore, the results indicate that at our working conditions no structured pore formation is taking place. The protein would trigger the liposome population aggregation before releasing the vesicle-entrapped ANTS, a molecule with a mass weight of only 427 Da.

FFEM. Changes in the mean size and shape of the liposome population were investigated by FFEM. We assume that the FFEM technique does not induce any change in the final determined particle size. Figure 6 shows the electron micrographs in the absence and presence of protein. Unilamellar vesicles of a mean diameter value of about 150−200 nm were visualized in the starting liposomes sample. The reaction mixture was analyzed at different incubation times, up to 30 min, at a 1:1000 and a 1:2000 protein/lipid molar ratio. The further analyzed 1:2000 protein/lipid ratio corresponds to a protein range where an aggregation activity is observed by DLS, but no leakage is detectable. This protein concentration is also below the threshold value, which leads to the ultimate formation of larger aggregates, liposome precipitation, and visible turbidity. Under these conditions, we detect by DLS an increase in the liposome population mean size up to about 300 nm. Frequent vesicle assemblies are visualized in the presence of protein. As a common feature, we can identify pairs of interacting liposomes, which are probably undergoing a partial-fusion process. Thus, morphological changes indicate a tendency of the LUV to aggregate. Detection of particles much smaller than the starting liposome mean size suggests that the process includes the release of some local lipid micelles. The observed small particles could represent regions of release of micelles from the lipid bilayer. In fact, the fragmentation of liposomes and release of small vesicles is also suggested by the reduction of turbidity assessed by the continuous optical density reading at 400 nm, when incubating the liposome suspension at a high protein concentration (data not shown).

DISCUSSION

The ECP is an eosinophil RNase involved in the immune innate system, with a described antipathogen activity. Antimicrobial properties have been reported for other RNase A family members, and it is suggested that the host defense function has been a key event in the family divergent evolution (*5*). Two eosinophil RNases, ECP and EDN, emerged via a gene duplication, and a strong evolutionary pressure would have promoted an increased cationicity and cytotoxicity for ECP (*6*−*8*). In fact, ECP divergence from the other eosinophil RNase (EDN) is considered as a reference example of one of the most rapid divergence events (*51*). Although eosinophils are mostly associated with parasitic infections, they can additionally participate in other antimicrobial activities (*13*). Besides, infiltration and local degranulation of eosinophils are observed into inflammation active sites, suggesting a key role in the inflammatory response (*14*). The eosinophil secretion granules contain several toxins, mainly ECP and the MBP, with described

antibacterial and membrane lytic activities, which would participate in the eosinophil immune defense system (*18*, *19*).

A common structural feature of most antibacterial protein and peptides is their amphiphilic character (*52*, *53*). The hydrophobic−hydrophilic balance is a crucial factor for lipid−peptide interactions (*37*) and is related to their antibacterial activity (*54*, *55*). The main target of antimicrobial peptides is the bacteria inner membrane, with a net negative charge (*25*, *56*, *57*). The interaction of the protein with the membrane would involve both hydrophobic interactions with the lipid acyl chain and electrostatic interactions between the positive residues and anionic phospholipid head groups (*58*, *59*).

We have previously reported a membrane destabilization capacity of ECP. A membrane lytic capacity has been related to the protein antibacterial activity and associated with the presence of the arginine residues and hydrophobic patches on the protein surface (*19*, *26*). We have now further analyzed the ECP membrane interaction mechanism on a synthetic lipid bilayer model. We observed the protein preference for anionic and zwitterionic phospholipids over neutral lipids. The results would provide a potential explanation of the mechanism of antimicrobial capacity, because anionic phospholipids are exposed on the external side of microbial membranes, while most anionic lipids are sequestred on the cytoplasmic side of the eukaryote host cell membrane. However, the protein preference for anionic lipids does not solely depend upon electrostatic interactions. Arginines have been found to play a key role in the cellular uptake of peptides, and specific interactions between the guanidinium groups of the arginines and the phosphate group of membrane lipids may be involved (*60*, *61*). A specific contribution of ECP arginine residues in the membrane association process is to be taken into account. ECP has accumulated an unusual number of Arg residues after a strong evolutionary pressure, with an isoelectric point (pI) close to 12. The high pI values of other RNase A family members, as angiogenin and rodent eosinophil-associated ribonucleases (EARs), might also be critical for their recently described antibacterial activity (*4*, *62*). A comparison of ECP activity on lipid vesicles of distinct composition indicates a preference for *E. coli* polar lipids versus DOPC/DOPG (3:2) vesicles (Figure 5). Even if the *E. coli* polar lipid extracts include phospholipids derived from both leaflets of the cytoplasmic membrane as well as the inner leaflet of the outer membrane, they are proven to be a good experimental model to assess the protein interactions with bacteria membranes (*63*).

We have also analyzed the topography of the ECP−membrane interaction by applying protein fluorescence techniques. The fluorescence properties of the wild-type protein were compared with single-Trp-containing mutants. To study the contribution of the W10 residue, mutants lacking the other Trp (W35) were constructed (W35A and W35AR36A). Data for the W35A single mutant was compared with the double-mutant construct, where the R36 neighboring residue is also substituted. The R36 side chain is packing against the Trp indole ring. Reciprocally, to analyze W35 contribution, the W10 residue was substituted (W10K construct). The W10 residue is located in the active site of RNase and can be involved in hydrogen-bond interactions. We have substituted W10 with its RNase A counterpart. All of the studied mutants do not alter the overall protein structural conformation and retain their enzymatic activity (*26*; S. Navarro, unpublished results). Besides, previous results obtained in our laboratory indicate that the protein membrane lytic and bactericidal activities are clearly dependent upon the W35 residue (*26*, *27*).

The classification of Trp residues obtained both by spectral and structural analysis is in excellent agreement. The data indicate that W10 and W35 belong to two distinct spectral and structural classes. W10 is an example of class I, represented by buried fluorophores in a relative nonpolar protein environment, while W35 belongs to class III, a class containing fully exposed fluorophores. The unusual exposure of W35 to the solvent reported for the ECP crystal structures in two different crystallization conditions (*34*, *35*) is also found in our experimental conditions, where the protein is in an aqueous solvent. In fact, the W35 solvent exposure at the protein surface will facilitate its membrane interaction capacity.

We can visualize the ECP association to the membrane by the Trp fluorescence spectra blue shift, observed immediately upon protein incubation with the liposomes (Tables 1 and 2 and Figure 2). No further changes in the fluorescence spectra are observed thereafter, suggesting that no slow translocation process is taking place. A close inspection of the wavelength maxima for WT ECP and both mutants at W10 and W35 shows that substitution of W10 does not substantially modify the protein spectra in the presence of liposomes, while the substitution of W35 eliminates the maximum wavelength displacement. We have also applied decomposition methods for the revealing of individual spectral components of WT ECP in the absence and presence of lipids. The results of the decomposition analysis (Table 2) are in a very good agreement with spectral data obtained on mutant proteins (Table 1). Decomposition analysis results corroborate the uneven contribution of both Trp residues to the final protein fluorescence emission spectra (Table 2). The data indicate that the recorded blue shift for ECP is, in fact, mostly due to the W35 penetration into the lipid bilayer.

Changes of the Trp environment properties upon membrane interaction were also studied by fluorescence quenching assays. When we incubate the protein in the presence of lipid vesicles, the solvent-exposed W35 residue is not accessible anymore to the iodide anion, suggesting that it is protected from the quencher by its association to the membrane. By comparing WT ECP Stern−Volmer plots with the mutants at W10 and W35 residues (Figure 3), we can deduce that most of the liposome-shielding effect takes place on the W35 residue. In fact, the W10K mutant, where we are only monitoring the quenching effect on W35, behaves very similarly to the wild-type protein, with a comparable calculated Stern−Volmer constant (K_{SV}). The same conclusions could be obtained from the results of the decomposition analysis (Table 2), which indicate that the value of the Stern−Volmer constant for the long-wavelength component attributed to W35 decreases several times as a result of the ECP interaction with liposomes.

The protein partial insertion into the lipid bilayer was further assessed by the quenching experiments using brominated lipids. The results are in agreement with the KI quenching data and indicate that ECP can partially insert into the membrane (Figure 4). The depth-dependent fluo-

rescence quenching experiment on both single Trp mutants suggests a depth location of about 9 Å from the lipid bilayer center for W35 and nearly no membrane insertion for W10. Registered wavelength displacement maxima for ECP and the W10K mutant in the presence of liposomes are in a wavelength range that suggests an interfacial location of W35 (*64*). The distance between Cα−Cα atoms of W35 and W10 residues calculated from the ECP crystallographic atomic structure is about 15 Å, and the minimum side-chain atom distance is about 10 Å (Figure 1). Therefore, the calculated distances would be in agreement with a protein partial-insertion process without any assumption about significant conformation structural changes in the protein. In fact, Trp residues might be responsible for the correct orientation of the protein in the lipid bilayer, preventing deep protein insertion into the membrane. Trp residues located in antibacterial peptides show a strong preference for the membrane interface (*65*), and in membrane proteins, they can fulfill a membrane interface anchoring function (*66*). Residue W35, exposed to the aqueous solvent at the ECP protein surface, would find itself in an unfavorable position and may tend to bury itself by interacting with a lipid bilayer. A close look at the ECP crystallographic dimer reported by ref *35* shows that W35 is located on the interacting interfaces of two ECP molecules. The dimer interface surface includes W35 together with discrete hydrophobic patches at the protein N-terminus and C-terminal loop. This protein surface hydrophobic contact area in an aqueous solvent media might tend to be hidden, either by interacting with another ECP molecule or, in the presence of liposomes, with the phospholipid bilayer.

We have further analyzed ECP activity over a wide protein concentration range. Our results indicate that ECP can destabilize the lipid bilayer at the nanomolar concentration range. ECP can induce liposome aggregation (Figure 5) before any significant vesicle content leakage is taking place (Table 4). The aggregation process has been followed by DLS (Figure 5) and confirmed by electron microscopy visualization (Figure 6). A combination of FFEM and DLS methodologies has allowed us to perform a thorough analysis of the effect of ECP on the size distribution of the liposome population. Analysis of electron microscope micrographs provides further information on the morphology of the liposome population. FFEM indicates that the protein can trigger the liposome aggregation and/or fusion process and suggests that the release of some lipid micelles is also taking place. Besides, in the assayed conditions, a partial-fusion process is also taking place, as assessed by the ANTS/DPX fusion assay (Cuyás et al., unpublished results). Aggregation of the liposome population is detectable at even a 2000 lipid/protein ratio (Figure 5B), and a significant liposome aggregation capacity is triggered from a threshold protein concentration (Figure 5C).

The data are compatible with a detergent or "carpet-like" mechanism for membrane destabilization. Moreover, the fact that the protein does not interact and/or destabilize neutral synthetic membranes also suggests a "carpet-like" mechanism, rather than a pore-forming mechanism. The lack of protein activity with neutral lipid bilayers [Figure 5 and previously reported leakage activity results (*26*)] indicates that hydrophobic interactions are not enough for the protein−membrane association and destabilization mechanism. The formation of transmembrane pores had once been described for ECP purified from mature eosinophils, at a higher protein concentration, and for a wide variety of lipid bilayers composition, including pure phosphatidylcholine (*67*). However, in our working conditions, we can rule out the formation of structured pores, because we observe a vesicle aggregation effect before any significant leakage of the vesicle-entrapped aqueous content is detectable. While the insertion of some peptides can be spontaneously driven mainly by the hydrophobic effect, the electrostatic attractions are needed for the peptides that require a surface association step before membrane insertion (*68*, *69*). According to the "carpet model", the protein would bind to the membrane surface until a threshold concentration is reached and then would be able to permeate it in a detergent-like manner (*57*). In fact, we do observe for ECP the onset of a liposome aggregation activity, from a threshold concentration, in the range of 100−200 nM (Figure 5), depending upon the vesicle composition. The increase of the vesicle population mean size shows a sigmoidal behavior in response to the protein concentration, suggesting a cooperative process (Figure 5). On the other hand, inspection of electron micrographs (Figure 6) reveals the presence of very small particles, which could represent the local release of lipid micelles, a process associated with the "carpet-like" model (*25*, *70*). In fact, the action at the bacteria cytoplasmic membrane by a "carpet-like" mechanism is the main process described for many antimicrobial molecules involved in the innate immune defense system. This mechanism provides a selective toxicity that discriminates between the host and microbial cells, a broad antimicrobial spectra, and a fast killing mechanism. The ECP activity on lipid bilayers could also explain some of the protein described secondary side effects reported in inflammation processes. The morphological changes observed on the surfactant ultrastructure upon incubation with ECP (*16*) could be explained by our results on the ECP capacity to fuse and lysate unilamellar vesicles. Hohlfeld and co-workers (*16*) observed by electron microscopy the ability of ECP to alter the pulmonary surfactant multilamellar layers.

To summarize, we can conclude that ECP has a potent membrane-destabilizing activity. The mechanism of action is dependent upon the lipid bilayer composition. The protein can aggregate the lipid vesicles before any significant leakage is taking place. Quenching topography experiments reveal that the protein can partially insert into the membrane and that the W35 residue would participate in the membrane association process. Our data are compatible with a detergent or "carpet-like" mechanism.

Although the synthetic lipid bilayers have proven to be a good working model, the final aim of our study is to identify the key structural determinants on the ECP-specific antimicrobial activity. We have previously proven that the protein membrane destabilization activity correlates with its antibacterial activity (*26*). However, results by site-directed mutagenesis on ECP activity on both Gram-negative and Gram-positive bacteria strains and a comparison with the protein cytotoxicity on eukaryotic cells indicate that specific interactions at the bacteria wall level should also be considered (*26*, *27*). In fact, antimicrobial proteins and peptides may not only have a membrane lytic activity but may also specifically interact with bacteria wall components (*71*). The widespread increase of bacterial resistance toward

many conventional antibiotics has led to the search for alternative drugs (*20*, *72*). Cationic proteins and peptides circulating in mammalian blood represent a source of host defense molecules that target the microbial wall and membranes (*13*). Our final goal is to analyze the structural parameters that determine the biological function of ECP as an eosinophil secretion protein involved in the innate immune defense system. ECP characterization would contribute to a better understanding of the function of antimicrobial proteins and their potential therapeutic use.

ACKNOWLEDGMENT

We acknowledge Núria Azemar, Departamento de Tensioactivos, CID, CSIC, Barcelona, Spain, for her assistance with the DLS measurements. FFTEM was performed by Carmen López at Serveis Científico−Tècnics, Parc Científic, Universitat de Barcelona, Barcelona, Spain. We also thank Edward Burstein for discussion.

REFERENCES

1. Venge, P., Bystrom, J., Carlson, M., Hakansson, L., Karawacjzyk, M., Peterson, C., Seveus, L., and Trulson, A. (1999) Eosinophil cationic protein (ECP): Molecular and biological properties and the use of ECP as a marker of eosinophil activation in disease, *Clin. Exp. Allergy 29*, 1172−1186.
2. Boix, E. (2001) Eosinophil cationic protein, *Methods Enzymol. 341*, 287−305.
3. Harder, J., and Schroder, J. M. (2002) RNase 7, a novel innate immune defense antimicrobial protein of healthy human skin, *J. Biol. Chem. 277*, 46779−46784.
4. Hooper, L. V., Stappenbeck, T. S., Hong, C. V., and Gordon, J. I. (2003) Angiogenins: A new class of microbicidal proteins involved in innate immunity, *Nat. Immunol. 4*, 269−273.
5. Cho, S., Beintema, J. J., and Zhang, J. (2005) The ribonuclease A superfamily of mammals and birds: Identifying new members and tracing evolutionary histories, *Genomics 85*, 208−220.
6. Rosenberg, H. F., and Dyer, K. D. (1995) Eosinophil cationic protein and eosinophil-derived neurotoxin. Evolution of novel function in a primate ribonuclease gene family, *J. Biol. Chem. 270*, 21539−21544.
7. Rosenberg, H. F., Dyer, K. D., Tiffany, H. L., and Gonzalez, M. (1995) Rapid evolution of a unique family of primate ribonuclease genes, *Nat. Genet. 10*, 219−223.
8. Bielawski, J. P., and Yang, Z. (2004) A maximum likelihood method for detecting functional divergence at individual codon sites, with application to gene family evolution, *J. Mol. Evol. 59*, 121−132.
9. Boix, E., Nikolovski, Z., Moiseyev, G. P., Rosenberg, H. F., Cuchillo, C. M., and Nogues, M. V. (1999) Kinetic and product distribution analysis of human eosinophil cationic protein indicates a subsite arrangement that favors exonuclease-type activity, *J. Biol. Chem. 274*, 15605−15614.
10. Rosenberg, H. F. (1995) Recombinant human eosinophil cationic protein. Ribonuclease activity is not essential for cytotoxicity, *J. Biol. Chem. 270*, 7876−7881.
11. Mancheno, J. M., Gasset, M., Onaderra, M., Gavilanes, J. G., and D'Alessio, G. (1994) Bovine seminal ribonuclease destabilizes negatively charged membranes, *Biochem. Biophys. Res. Commun. 199*, 119−124.
12. Muller, C. A., Autenrieth, I. B., and Peschel, A. (2005) Innate defenses of the intestinal epithelial barrier, *Cell. Mol. Life Sci. 62*, 1297−1307.
13. Levy, O. (2000) Antimicrobial proteins and peptides of blood: Templates for novel antimicrobial agents, *Blood 96*, 2664−2672.
14. Gleich, G. J. (2000) Mechanisms of eosinophil-associated inflammation, *J. Allergy Clin. Immunol. 105*, 651−663.
15. Davis, M. D., Plager, D. A., George, T. J., Weiss, E. A., Gleich, G. J., and Leiferman, K. M. (2003) Interactions of eosinophil granule proteins with skin: Limits of detection, persistence, and vasopermeabilization, *J. Allergy Clin. Immunol. 112*, 988−994.
16. Hohlfeld, J. M., Schmiedl, A., Erpenbeck, V. J., Venge, P., and Krug, N. (2004) Eosinophil cationic protein alters pulmonary surfactant structure and function in asthma, *J. Allergy Clin. Immunol. 113*, 496−502.
17. Tai, P. C., Spry, C. J., Peterson, C., Venge, P., and Olsson, I. (1984) Monoclonal antibodies distinguish between storage and secreted forms of eosinophil cationic protein, *Nature 309*, 182−184.
18. Abu-Ghazaleh, R. I., Gleich, G. J., and Prendergast, F. G. (1992) Interaction of eosinophil granule major basic protein with synthetic lipid bilayers: A mechanism for toxicity, *J. Membr. Biol. 128*, 153−164.
19. Lehrer, R. I., Szklarek, D., Barton, A., Ganz, T., Hamann, K. J., and Gleich, G. J. (1989) Antibacterial properties of eosinophil major basic protein and eosinophil cationic protein, *J. Immunol. 142*, 4428−4434.
20. Zasloff, M. (2002) Antimicrobial peptides of multicellular organisms, *Nature 415*, 389−395.
21. Lohner, K., and Blondelle, S. E. (2005) Molecular mechanisms of membrane perturbation by antimicrobial peptides and the use of biophysical studies in the design of novel peptide antibiotics, *Comb. Chem. High Throughput Screening 8*, 241−256.
22. Dathe, M., Meyer, J., Beyermann, M., Maul, B., Hoischen, C., and Bienert, M. (2002) General aspects of peptide selectivity towards lipid bilayers and cell membranes studied by variation of the structural parameters of amphipathic helical model peptides, *Biochim. Biophys. Acta 1558*, 171−186.
23. Ericksen, B., Wu, Z., Lu, W., and Lehrer, R. I. (2005) Antibacterial activity and specificity of the six human α-defensins, *Antimicrob. Agents Chemother. 49*, 269−275.
24. Ambroggio, E. E., Separovic, F., Bowie, J. H., Fidelio, G. D., and Bagatolli, L. A. (2005) Direct visualization of membrane leakage induced by the antibiotic peptides: Maculatin, citropin, and aurein, *Biophys. J. 89*, 1874−1881.
25. Papo, N., and Shai, Y. (2005) Host defense peptides as new weapons in cancer treatment, *Cell. Mol. Life Sci. 62*, 784−790.
26. Carreras, E., Boix, E., Rosenberg, H. F., Cuchillo, C. M., and Nogues, M. V. (2003) Both aromatic and cationic residues contribute to the membrane-lytic and bactericidal activity of eosinophil cationic protein, *Biochemistry 42*, 6636−6644.
27. Carreras, E., Boix, E., Navarro, S., Rosenberg, H. F., Cuchillo, C. M., and Nogues, M. V. (2005) Surface-exposed amino acids of eosinophil cationic protein play a critical role in the inhibition of mammalian cell proliferation, *Mol. Cell. Biochem. 272*, 1−7.
28. Motojima, S., Frigas, E., Loegering, D. A., and Gleich, G. J. (1989) Toxicity of eosinophil cationic proteins for guinea pig tracheal epithelium in vitro, *Am. Rev. Respir. Dis. 139*, 801−805.
29. Fredens, K., Dybdahl, H., Dahl, R., and Baandrup, U. (1988) Extracellular deposit of the cationic proteins ECP and EPX in tissue infiltrations of eosinophils related to tissue damage, *Acta Pathol. Microbiol. Immunol. Scand. 96*, 711−719.
30. Humbles, A. A., Lloyd, C. M., McMillan, S. J., Friend, D. S., Xanthou, G., McKenna, E. E., Ghiran, S., Gerard, N. P., Yu, C., Orkin, S. H., and Gerard, C. (2004) A critical role for eosinophils in allergic airways remodeling, *Science 305*, 1776−1779.
31. Reshetnyak, Y. K., Koshevnik, Y., and Burstein, E. A. (2001) Decomposition of protein tryptophan fluorescence spectra into log-normal components. III. Correlation between fluorescence and microenvironment parameters of individual tryptophan residues, *Biophys. J. 81*, 1735−1758.
32. Burstein, E. A., and Emelyanenko, V. I. (1996) Log-normal description of fluorescence spectra of organic fluorophores, *Photochem. Photobiol. 64*, 316−320.
33. Burstein, E. A., Abornev, S. M., and Reshetnyak, Y. K. (2001) Decomposition of protein tryptophan fluorescence spectra into log-normal components. I. Decomposition algorithms, *Biophys. J. 81*, 1699−1709.
34. Boix, E., Leonidas, D. D., Nikolovski, Z., Nogues, M. V., Cuchillo, C. M., and Acharya, K. R. (1999) Crystal structure of eosinophil cationic protein at 2.4 Å resolution, *Biochemistry 38*, 16794−16801.
35. Mallorqui-Fernandez, G., Pous, J., Peracaula, R., Aymami, J., Maeda, T., Tada, H., Yamada, H., Seno, M., de Llorens, R., Gomis-Ruth, F. X., and Coll, M. (2000) Three-dimensional crystal structure of human eosinophil cationic protein (RNase 3) at 1.75 Å resolution, *J. Mol. Biol. 300*, 1297−1307.
36. Mohan, C. G., Boix, E., Evans, H. R., Nikolovski, Z., Nogues, M. V., Cuchillo, C. M., and Acharya, K. R. (2002) The crystal structure of eosinophil cationic protein in complex with 2′,5′-ADP at 2.0 Å resolution reveals the details of the ribonucleolytic active site, *Biochemistry 41*, 12100−12106.

37. Kitamura, A., Kiyota, T., Tomohiro, M., Umeda, A., Lee, S., Inoue, T., and Sugihara, G. (1999) Morphological behavior of acidic and neutral liposomes induced by basic amphiphilic α-helical peptides with systematically varied hydrophobic−hydrophilic balance, *Biophys. J. 76*, 1457−1468.
38. Reshetnyak, Y. K., and Burstein, E. A. (2001) Decomposition of protein tryptophan fluorescence spectra into log-normal components. II. The statistical proof of discreteness of tryptophan classes in proteins, *Biophys. J. 81*, 1710−1734.
39. Ladokhin, A. S. (1999) Analysis of protein and peptide penetration into membranes by depth-dependent fluorescence quenching: Theoretical considerations, *Biophys. J. 76*, 946−955.
40. McIntosh, T. J., and Holloway, P. W. (1987) Determination of the depth of bromine atoms in bilayers formed from bromolipid probes, *Biochemistry 26*, 1783−1788.
41. Bartlett, G. R. (1959) Colorimetric assay methods for free and phosphorylated glyceric acids, *J. Biol. Chem. 234*, 469−471.
42. Johnsen, R. M. (1992) *Light Scattering in Biochemistry*, The Royal Society of Chemistry, Cambridge, U.K.
43. López, O., López-Iglesias, C., Cócera, M., Walther, P., Parra, J. L., and de la Maza, A. (2004) Influence of chemical and freezing fixation methods in the freeze-fracture of stratum corneum, *J. Struct. Biol. 146*, 302−309.
44. Egelhaaf, S. U., Wehrli, E., Müller, M., Adrian, M., and Schurtenberger, P. (1996) Determination of the size distribution of lecithin liposomes: A comparative study using freeze fracture, cryoelectron microscopy and dynamic light scattering, *J. Microsc. 184*, 214−228.
45. Krissinel, E., and Henrick, K. (2005) *Detection of Protein Assemblies in Crystals*, Vol. LNBI 3695, Springer-Verlag, Berlin, Germany.
46. Sanjeev, B. S., and Vishveshwara, S. (2004) Conformational transitions in eosinophil cationic protein: A molecular dynamics study in aqueous environment, *J. Biomol. Struct. Dyn. 22*, 171−182.
47. Lehrer, S. S. (1971) Solute perturbation of protein fluorescence. The quenching of the tryptophyl fluorescence of model compounds and of lysozyme by iodide ion, *Biochemistry 10*, 3254−3263.
48. Lakowicz, J. R. (1983) *Principles of Fluorescence Spectroscopy*, Plenum Press, New York.
49. Markello, T., Zlotnick, A., Everett, J., Tennyson, J., and Holloway, P. W. (1985) Determination of the topography of cytochrome b_5 in lipid vesicles by fluorescence quenching, *Biochemistry 24*, 2895−2901.
50. Thoren, P. E., Persson, D., Esbjorner, E. K., Goksor, M., Lincoln, P., and Norden, B. (2004) Membrane binding and translocation of cell-penetrating peptides, *Biochemistry 43*, 3471−3489.
51. Zhang, J., Rosenberg, H. F., and Nei, M. (1998) Positive Darwinian selection after gene duplication in primate ribonuclease genes, *Proc. Natl. Acad. Sci. U.S.A. 95*, 3708−3713.
52. Hilpert, K., Volkmer-Engert, R., Walter, T., and Hancock, R. E. (2005) High-throughput generation of small antibacterial peptides with improved activity, *Nat. Biotechnol. 23*, 1008−1012.
53. Sitaram, N., and Nagaraj, R. (1999) Interaction of antimicrobial peptides with biological and model membranes: Structural and charge requirements for activity, *Biochim. Biophys. Acta 1462*, 29−54.
54. Oren, Z., and Shai, Y. (1997) Selective lysis of bacteria but not mammalian cells by diastereomers of melittin: Structure−function study, *Biochemistry 36*, 1826−1835.
55. Brown, K. L., and Hancock, R. E. (2006) Cationic host defense (antimicrobial) peptides, *Curr. Opin. Immunol. 18*, 24−30.
56. Hancock, R. E., and Chapple, D. S. (1999) Peptide antibiotics, *Antimicrob. Agents Chemother. 43*, 1317−1323.
57. Papo, N., and Shai, Y. (2003) Can we predict biological activity of antimicrobial peptides from their interactions with model phospholipid membranes? *Peptides 24*, 1693−1703.
58. Reynaud, J. A., Grivet, J. P., Sy, D., and Trudelle, Y. (1993) Interactions of basic amphiphilic peptides with dimyristoylphosphatidylcholine small unilamellar vesicles: Optical, NMR, and electron microscopy studies and conformational calculations, *Biochemistry 32*, 4997−5008.
59. Yoshimura, T., Goto, Y., and Aimoto, S. (1992) Fusion of phospholipid vesicles induced by an amphiphilic model peptide: Close correlation between fusogenicity and hydrophobicity of the peptide in an α-helix, *Biochemistry 31*, 6119−6126.
60. Kaznessis, Y. N., Kim, S., and Larson, R. G. (2002) Specific mode of interaction between components of model pulmonary surfactants using computer simulations, *J. Mol. Biol. 322*, 569−582.
61. Thoren, P. E., Persson, D., Lincoln, P., and Norden, B. (2005) Membrane destabilizing properties of cell-penetrating peptides, *Biophys. Chem. 114*, 169−179.
62. Ishihara, K., Asai, K., Nakajima, M., Mue, S., and Ohuchi, K. (2003) Preparation of recombinant rat eosinophil-associated ribonuclease-1 and -2 and analysis of their biological activities, *Biochim. Biophys. Acta 1638*, 164−172.
63. White, G. F., Racher, K. I., Lipski, A., Hallett, F. R., and Wood, J. M. (2000) Physical properties of liposomes and proteoliposomes prepared from *Escherichia coli* polar lipids, *Biochim. Biophys. Acta 1468*, 175−186.
64. Wimley, W. C., and White, S. H. (2000) Determining the membrane topology of peptides by fluorescence quenching, *Biochemistry 39*, 161−170.
65. Yau, W. M., Wimley, W. C., Gawrisch, K., and White, S. H. (1998) The preference of tryptophan for membrane interfaces, *Biochemistry 37*, 14713−14718.
66. Ridder, A. N., Morein, S., Stam, J. G., Kuhn, A., de Kruijff, B., and Killian, J. A. (2000) Analysis of the role of interfacial tryptophan residues in controlling the topology of membrane proteins, *Biochemistry 39*, 6521−6528.
67. Young, J. D., Peterson, C. G., Venge, P., and Cohn, Z. A. (1986) Mechanism of membrane damage mediated by human eosinophil cationic protein, *Nature 321*, 613−616.
68. Liu, L. P., and Deber, C. M. (1997) Anionic phospholipids modulate peptide insertion into membranes, *Biochemistry 36*, 5476−5482.
69. Powers, J. P., Tan, A., Ramamoorthy, A., and Hancock, R. E. (2005) Solution structure and interaction of the antimicrobial polyphemusins with lipid membranes, *Biochemistry 44*, 15504−15513.
70. Shai, Y. (1999) Mechanism of the binding, insertion and destabilization of phospholipid bilayer membranes by α-helical antimicrobial and cell non-selective membrane-lytic peptides, *Biochim. Biophys. Acta 1462*, 55−70.
71. Gabay, J. E. (1994) Ubiquitous natural antibiotics, *Science 264*, 373−374.
72. D'Costa, V. M., McGrann, K. M., Hughes, D. W., and Wright, G. D. (2006) Sampling the antibiotic resistome, *Science 311*, 374−377.

BI061190E